Scalar, tensor, and vector polarizability of Tm atoms in a 532-nm dipole trap

V. V. Tsyganok,[1,2] D. A. Pershin,[1,2] E. T. Davletov,[1,2] V. A. Khlebnikov,[1] and A. V. Akimov[1,3,4,*]

[1]*Russian Quantum Center, Business Center "Ural," 100A Novaya Str., Skolkovo, Moscow 143025, Russia*

[2]*Moscow Institute of Physics and Technology, Institutskii per. 9, Dolgoprudny, Moscow Region 141701, Russia*

[3]*PN Lebedev Institute RAS, Leninsky Prospekt 53, Moscow 119991, Russia*

[4]*Texas A&M University, 4242 TAMU, College Station, Texas 77843, USA*

(Received 9 May 2019; revised manuscript received 10 July 2019; published 4 October 2019)

Dipolar atoms have unique properties, making them interesting for laser cooling and quantum simulations. But, due to relatively large orbital momentum in the ground state these atoms may have large dynamic tensor and vector polarizabilities in the ground state. This enables the formation of spin-dependent optical traps. In this paper the real part of tensor and vector dynamic polarizability was experimentally measured and compared to a theoretical simulation. For an optical dipole trap operating around 532.07 nm, tensor polarizability was found to be -145 ± 53 a.u. and vector polarizability was 680 ± 240 a.u. The measurements were compared with simulations, which were done based on the known set of levels from a thulium atom. The simulations are in good agreement with experimental results. In addition, losses of atoms from the dipole trap were measured for different trap configurations and compared to the calculated imaginary part of vector and tensor polarizabilities.

DOI: 10.1103/PhysRevA.100.042502

I. INTRODUCTION

Ultracold atoms have high potential in the field of quantum simulations [1–3]. One of the key advantages of cold atomic ensembles is a large degree of control over interatomic interactions as well as the internal states of an atom [4]. Among other elements, the rare earths hold a special place on the periodic table as they have incomplete electronic f shells and therefore also have high orbital and magnetic moments in the ground state. This affects many properties of rare-earth elements, including a large number of Feshbach resonances in low fields [5,6] and strong dipole-dipole interactions [7–11].

Another important degree of control enabled with rare-earth elements is their highly anisotropic polarizability in a wide range of light spectrum, which is already well manifested even for the atomic ground state.

Dynamic polarizability is an important property of an atom, to a high degree determining the interaction of an atom with a nonresonant light field. Alkali atoms are known to have mostly scalar polarizability in the ground state due to an s-type electronic shell in the ground state. To the contrary, rare-earth elements have a nonzero orbital momentum in the ground state. This gives rise to considerable contribution of the tensor and vector polarizabilities—-even in the ground state. In particular, polarizabilities for the erbium atom were recently calculated [12] and measured experimentally [13].

In this paper we experimentally study the dynamic polarizabilities of cold thulium atoms in a 532-nm dipole trap [14]. By manipulating the orientation of atomic ensemble polarization and polarization of the light field, we were able to extract tensor and vector components of the dynamic polarizability and compare them with simulations based on known transitions in thulium atoms [15]. We demonstrate that around this wavelength contributions of tensor and vector polarizability are quite significant, thus allowing formation of spin-dependent traps. Besides this, we also specifically analyzed losses from the atomic trap depending on the mutual orientation of atomic polarization and light polarization and compared them with our simulations. We found that losses do not follow the behavior of the imaginary part of polarizability, thus we excluded the simplest radiative loss mechanism for our trap.

II. SIMULATIONS

In the presence of a nonresonant light field of frequency ω, atomic energy levels undergo shift leading to trapping potential $U(\omega)$. It could be expressed as the sum of the scalar U_s, vector U_υ, and tensor U_t parts [16] as follows [13]:

$$
\begin{aligned}
U(\omega) &= -\frac{1}{2\varepsilon_0 c} I(r)\mathrm{Re}[\alpha_{\mathrm{tot}}] = U_s + U_\upsilon + U_t \\
U_s &= -\frac{1}{2\varepsilon_0 c} I(r)\mathrm{Re}[\alpha_s(\omega)] \\
U_\upsilon &= -\frac{1}{2\varepsilon_0 c} I(r)\varepsilon\, \cos\theta_k \frac{m_F}{2F}\,\mathrm{Re}[\alpha_\upsilon(\omega)] \\
U_t &= -\frac{1}{2\varepsilon_0 c} I(r)\frac{3m_F^2 - F(F+1)}{F(2F-1)}\frac{3\cos^2\theta_p - 1}{2}\mathrm{Re}[\alpha_t(\omega)],
\end{aligned}
\tag{1}
$$

where ε_0 is the vacuum permittivity; c is the speed of light; $I(r)$ is the laser intensity profile; $\varepsilon = |\vec{u}^* \times \vec{u}|$ is the ellipticity parameter with $\vec{u}$ the normalized Jones vector; $\theta_p = \angle(\vec{E}, \vec{B})$ and $\theta_k = \angle(\vec{k}, \vec{B})$ [see Fig. 1(a)]; F is the total angular momentum quntum number inclusive of nuclear spin; m_F is the total angular-momentum projection quantum number;

*akimov@physics.tamu.edu

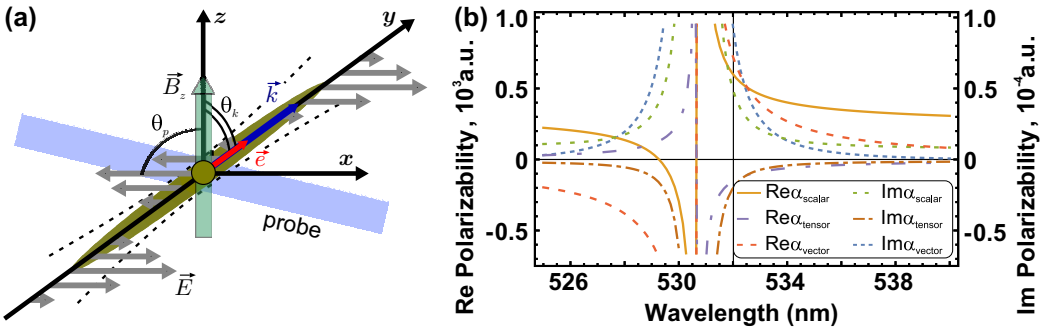

FIG. 1. (a) Idea of the experiment: polarized atomic cloud (orientated always along magnetic field) in a single-beam ODT with elliptical polarization that is propagated along the y axis ($\vec{e}$ vector). (b) Real and imaginary parts of ground-state polarizabilities in the region of 532.07-nm laser light. The black vertical line is the wavelength of our ODT.

$\alpha_{\rm tot}$ is the total atomic polarizability; $\alpha_s(\omega)$, $\alpha_v(\omega)$, $\alpha_t(\omega)$ are scalar, vector, and tensor dynamic dipole polarizabilities, respectively.

Imaginary parts of polarization values set photon scattering rates that are given by a similar expression:

$$\Gamma(\omega) = \frac{1}{\hbar\varepsilon_0 c} I(r)\Big[\mathrm{Im}[\alpha_s(\omega)] + \varepsilon\,\cos\theta_k\,\frac{m_F}{2F}\,\mathrm{Im}[\alpha_v(\omega)] + \frac{3m_F^2 - F(F+1)}{F(2F-1)} \times \frac{3\cos^2\theta_p - 1}{2}\mathrm{Im}[\alpha_t(\omega)]\Big]. \tag{2}$$

To calculate all parts of dynamic dipole polarizability, we follow the sum-over-state approach (see Appendix A). Energy levels and corresponding natural linewidths for dipole-allowed transitions were taken from the National Institute of Standard (NIST) database [15].

Figure 1(b) depicts calculated values of the thulium atom's real and imaginary parts of ground-state polarizabilities in the region of 532 nm. The experimentally measured wavelength of the optical dipole trap (ODT) light was found to be 532.07 nm (using Wavelength Meter WS-7, calibrated by the thulium transition line). For this wavelength the simulation gives values of 583, 684, and -140 a.u. for real parts of scalar, vector, and tensor polarizabilities, respectively; imaginary parts are 446×10^{-7} a.u., 836×10^{-7} a.u., and 183×10^{-7} a.u., respectively. These quantities are strongly affected by the near-lying 530.7-nm optical transition with a level's width of 345 kHz. Thus, it was found that vector and tensor part are almost entirely formed by this transition, while for scalar polarizability it provides about half of the value.

III. EXPERIMENT

To measure the polarizability of thulium at a wavelength of 532.07 nm, an atomic cloud of ^{169}Tm was initially cooled down with a magneto-optical trap (MOT) [14]. In this type of MOT, the atomic cloud is spin polarized to the lowest ground-state Zeeman sublevel ($J = 7/2$, $F = 4$, $m_F = -4$) with a population of $m_F = -4$ higher than 97%. Atoms were then loaded to ODT and maintained in the magnetic field of 3.91 G [17]. The hyperfine splitting of the ground state of thulium atom is around 1.5 GHz (nuclear spin is 1/2) and is larger than any ground-state related energy scale in the frame of this paper. The residual gradient of magnetic field in the ODT region was estimated via microwave experiment [18] and does not exceed 40 mG/cm. Then atoms were transferred into a single-beam optical dipole trap [19] operating at 532.07 nm, formed by Verdy-V10 laser (Coherent Inc.) with a specified spectral linewidth of 5 MHz. After 300 ms of holding time in the ODT, about 1.5×10^6 atoms with a temperature of around 18 μK were typically achieved with vertical orientation of the magnetic field [along the z axis in Fig. 1(a) and linear horizontal polarization of the ODT beam $\theta_k \approx \theta_p \approx 90^\circ$. Corresponding density of atoms could be estimated as approximately $1.5 \times 10^{12}\mathrm{cm}^{-3}$. To detect the atomic cloud, the absorption imaging technique was used [20]. For this purpose, imaging beam locked in its frequency to atomic resonance was used. The beam was in the xz plane making 16° angle with the x axis [see Fig. 1(a)].

In some experiments, θ_p was varied by changing currents in the magnetic-field coils, thus turning the direction of the magnetic field. This rotation was performed after the light of MOT had been switched off. We were able to control the magnetic-field values with 50-mG precision accuracy [17]. For angles different from $\theta_k \approx \theta_p \approx 90^\circ$, the depth of the dipole trap changes greatly due to the presence of tensor and vector polarizabilities [see Fig. 2(a) and Eq. (1)]. Thus, after such a rotation, the number of atoms as well as the temperature of the atomic cloud in the ODT varies greatly depending on the rotation angle. However, even in the worst condition for the ODT ($\theta_k = 90^\circ$, $\theta_p = 0^\circ$), we had enough atoms to perform an experiment. To understand the depth of the ODT U, the standard technique of trap-frequency measurements was used [13]. The total polarizability, $\alpha_{\rm tot}$, then could be found using Eq. (1). For the Gaussian beam which propagates along the y axis the intensity profile is

$$I(x,z) = I_0\,\exp\left[-\frac{2x^2}{w_x^2} - \frac{2z^2}{w_z^2}\right], \tag{3}$$

where w_x and w_z are beam waists, and $I_0 = 2P/\pi w_x w_z$, where P is beam power. The trap frequencies in harmonic

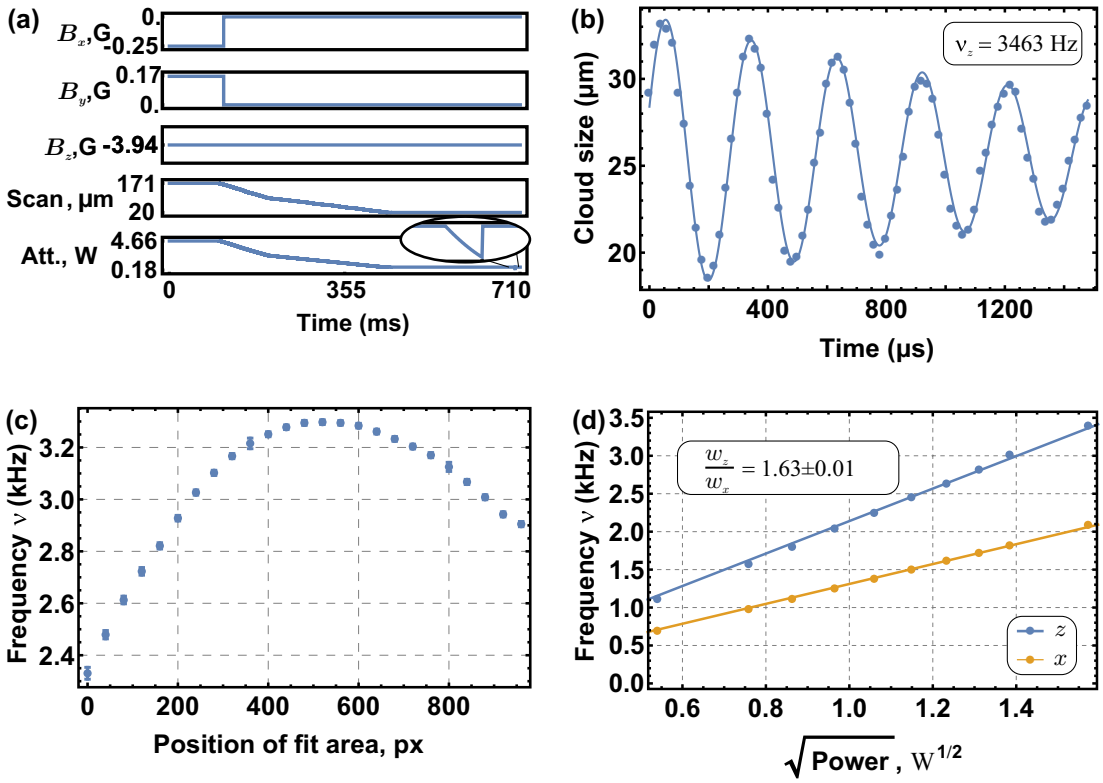

FIG. 2. (a) Scheme of pulses used in the experiment with tensor polarization. (b) Typical fit of atomic cloud size oscillations in the z direction versus time. (c) Dependence of fitted frequency vs position of fit. (d) Frequency vs square root of ODT beam power (without sweeping) for both radial x- and z axes.

approximation ν_i could be then calculated as [19]

$$\nu_i = \frac{1}{2\pi}\sqrt{\frac{-4\,U_0}{m_{Tm}\,w_i^2}}, \quad i \in \{x, z\}$$
$$\nu_y = \frac{1}{2\pi}\sqrt{\frac{-2U_0}{m_{Tm}\,w_y^2}}, \tag{4}$$

where m_{Tm} is the atomic mass, w_y is Rayleigh length, and $U_0 = -\alpha_{\rm tot}\, I_0/2\varepsilon_0 c$. Thus, using (4) one can find expression for total polarizability via parameters, measured in the experiment:

$$\alpha_{\rm tot} = \pi^3\varepsilon_0 c\frac{\nu_x^2 w_x^3 w_z m_{Tm}}{P} = \pi^3\varepsilon_0 c\frac{\nu_z^2 w_z^3 w_x m_{Tm}}{P}. \tag{5}$$

A. Frequency measurements

To measure the ODT frequency, an atomic cloud was kept in the ODT for 300 ms after ODT sweeping was turned off [17]. After this time, evaporative cooling mostly stops and atoms can be considered thermalized. At this point, the atoms occupied the central part of the trap. The power of the beam was then decreased by four times over 2 ms, followed by a sharp increase to the required value of power, thereby causing oscillations of atomic cloud size and position [Fig. 2(b)].

Since the ODT was formed by a single Gaussian beam, the frequency of oscillations depends on the fitted region along the beam. Therefore, we divided the experimental images into 25 parts of 40 pixels each. For each region the frequency was fitted [see Fig. 2(b)] and plotted versus position along the beam [Fig. 2(c)]. The maximum frequency found this way was used for calculating the trap frequency, which is 1/2 of the trap oscillation frequency.

B. Beam waist

To measure the ODT waists, we used a CMOS Thorlabs DCU223M-GL camera by placing it into the laser beam reflected with an additional mirror in front of the vacuum chamber. The problem was that the size of the laser spot occupied a small number of camera pixels, resulting in a large inaccuracy of ODT waists. To overcome this, we performed our measurement with a sweeping trap [17], which has an increased waist along the x direction. Another waist can be reconstructed from ODT frequencies with Eq. (4):

$$\frac{-4\,U_0}{m_{Tm}(2\pi)^2} = \nu_x^2 w_x^2 = \nu_z^2 w_z^2 = 2\nu_y^2 w_y^2. \tag{6}$$

The waist of the sweeping ODT along the x direction is shown in Fig. 3(a). The sweeping shape was designed to make the beam profile parabolic [17] near its maximum. The position of the camera was scanned around the location of the focal spot to find the minimal beam size. Due to the large size of the swept beam, the laser spot occupied a large number of pixels. Its size was mostly determined by the sweeping amplitude rather than the quality of beam focusing; thus, we excluded possible aberrations on the vacuum window

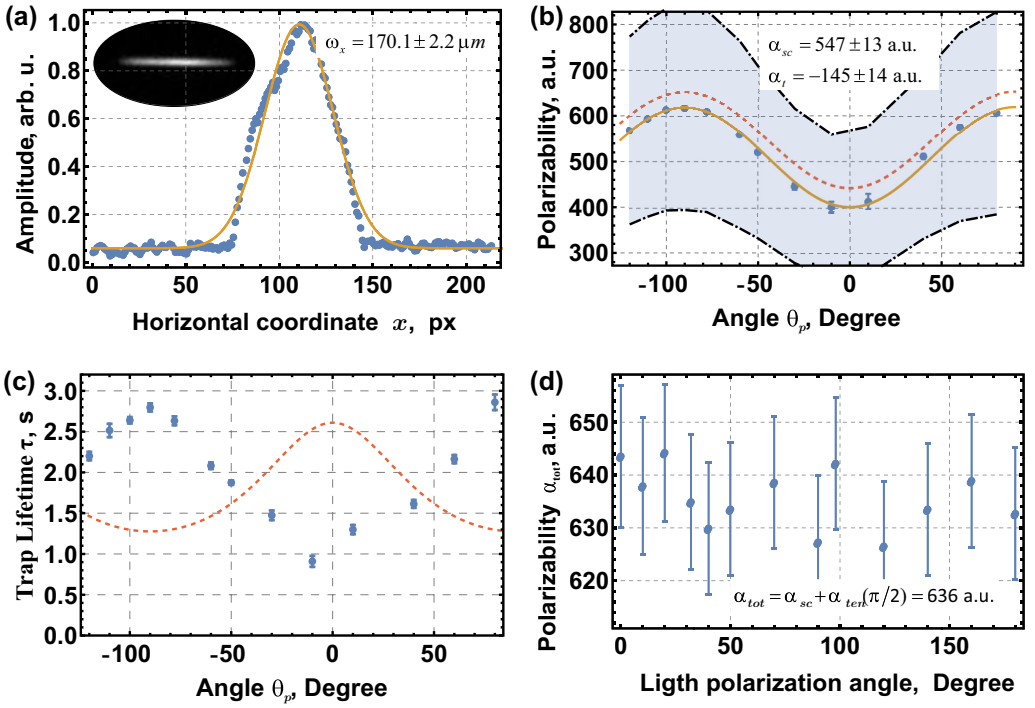

FIG. 3. (a) Sweeping trap profile (beam intensity was time averaged during imaging): dots represent intensity averaged by y dimension, solid yellow line represents Gaussian fit. (b) Atomic polarizability vs θ_p. Gray area with dot-dashed borders illustrates systematic uncertainty of the measurements. Solid yellow line represents fit of the experimental data with sine dependence; dashed red line represents the simulations of the real part of the polarizability. (c) Lifetime of atoms in the dipole trap vs θ_p. Dashed red line represents normalized and inversed calculated imaginary part of the polarizability. (d) Atomic polarizability vs the linear light polarization angle. In this experiment the magnetic field was codirected with the ODT beam and $\theta_k = 0^\circ$. For all plots error bars indicate statistical uncertainty only. For systematic uncertainties, please see Appendix C.

and the additional mirror. The fit of the intensity profile measured this way returned a value for the beam width in the x direction of $w_{x\ \text{sweeping mode on}} = 170 \pm 2_{\text{stat}}\mu m$. Here and below we mark statistical uncertainty by the index *stat*. The effective waist of the one-dimensional (1D) brightness profile of the swept beam [Fig. 3(a)] gave a value of $189\,\mu m$ (see Appendix B for details). Thus, we estimated error related to the difference between the observed swept beam profile and the Gaussian profile to be $19\mu m$. Finally, $w_{x\ \text{sweeping mode on}} = 170 \pm 19\mu m$.

Given this linear dimension, the rest of the measurements can be done via measurements of trap frequencies. The frequencies of the ODT were measured by the method described in the Frequency Measurements section. The frequency measurements were done in two configurations: one with sweeping in the x-beam direction, and one without. In the latter case, intensity of the trap beam was reduced by a factor of 6.3 times. This was done to avoid heating during turning off the sweeping. As a result the following frequencies were measured:

$$\begin{aligned}
\nu_{x\ \text{sweeping mode on}} &= 157 \pm 3_{\text{stat}}\ \text{Hz} \\
\nu_{z\ \text{sweeping mode on}} &= 1649 \pm 6_{\text{stat}}\ \text{Hz} \\
\nu_{x\ \text{sweeping mode off}} &= 981 \pm 6_{\text{stat}}\ \text{Hz} \\
\nu_{z\ \text{sweeping mode off}} &= 1560 \pm 8_{\text{stat}}\ \text{Hz}.
\end{aligned} \tag{7}$$

Here error bars are statistical errors. Using Eq. (6) the parameters of the beam were found to be

$$\begin{aligned}
w_x &= w_{x\ \text{sweeping mode on}} \cdot \frac{\nu_{x\ \text{sweeping mode on}}}{\nu_{x\ \text{sweeping mode off}}} \cdot \frac{\nu_{z\ \text{sweeping mode off}}}{\nu_{z\ \text{sweeping mode on}}} \\
&= 25.7 \pm 3.5_{\text{stat}}\ \mu\text{m} \\
w_z &= w_x \cdot \frac{\nu_{x\ \text{sweeping mode off}}}{\nu_{z\ \text{sweeping mode off}}} = 15.8 \pm 2.3_{\text{stat}}\ \mu\text{m}.
\end{aligned} \tag{8}$$

Finally, we measured the dependences of the frequencies in the two orthogonal directions versus power without sweeping regime [Fig. 2(d)]. The ratio between the found parameters w_x and w_z is constant with power much as was expected: $w_z/w_x = 1.63 \pm 0.01_{\text{stat}}$.

C. Tensor and scalar polarizability

As it can be seen from Eq. (1), when $\theta_k = 90^\circ$ or when the ellipticity parameter $\varepsilon = |\vec{u}^* \times \vec{u}| = 0$ (ODT beam linear polarized) then the vector term in (1) becomes zero and therefore

$$\alpha_{\text{tot}} = \alpha_{sc} + \frac{3m_F^2 - F(F+1)}{F(2F-1)} \times \frac{3\cos^2\theta_p - 1}{2}\alpha_t. \tag{9}$$

The angle θ_k was varied by adiabatic change of an external magnetic field governing atom orientation. Orientation of the magnetic field was calibrated with microwave spectroscopy [18]. In addition, the ODT beam polarization was cleaned by a polarization beam splitter in combination with a $\lambda/4$ plate

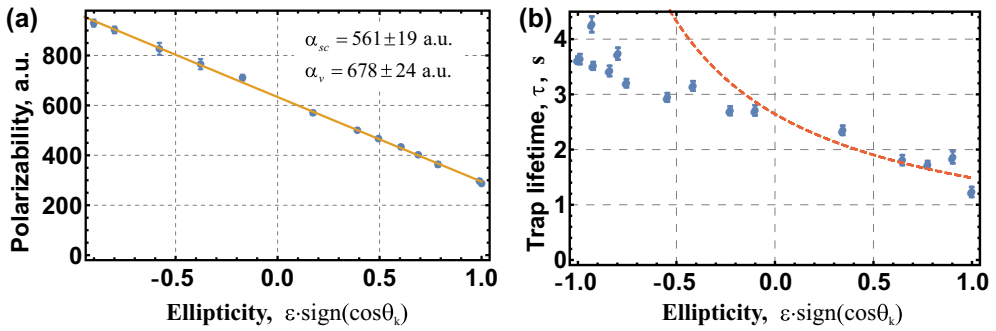

FIG. 4. (a) Dependence of the atomic polarizability versus the ellipticity parameter and sign of circular polarization. At this experiment $\theta_k \approx 0^\circ$. Error bars contain statistical uncertainty only. (b) Lifetime of the ODT versus ellipticity of the trap beam. Red dashed line indicates the normalized, inversed imaginary part of the polarizability.

and thus the ellipticity parameter, $\varepsilon = |\vec{u}^* \times \vec{u}|$, was less than 0.03 during all the measurements.

To measure the tensor part of the polarizability, we used a linearly polarized ODT varying angle θ_p [see Fig. 3(b)]. Orientation of the ODT polarization was controlled by a half-lambda plate. For each position of the $\lambda/2$ plate, the ODT was loaded as described above and frequency of ODT in the z direction was measured (see Frequency Measurements). Polarization of the beam was checked by polarization beam splitter (PBS) placed after the vacuum chamber. The polarizability was calculated from measured frequencies using Eqs. (5) and (9): $\alpha_{sc} = 547 \pm 51$ a.u., $\alpha_t = -145 \pm 14$ a.u. (see Appendix C for details of error calculations). While there is good agreement between experimental and calculated values of tensor polarizability, the scalar part is slightly lower than the calculated value. We dedicate this deviation to systematic errors in the determination of the beam waist and its anharmonicity. We note that while influence of the lack of the spectroscopic data may affect calculated value, the absent spectroscopic data is likely to be in the ultraviolet part of the spectrum, corresponding to transitions from rather high energy levels and therefore can only increase calculated value, but not shift it towards measured value.

Besides measurements of polarizability, the lifetime of thulium atoms in the ODT was measured versus θ_p [see Fig. 3(c)]. The lifetime was extracted from decay of the number of atoms in ODT by fitting the curve with exponential dependence. One could see that lifetime mostly follows the real part of the polarizability. Here we see that surprisingly the lifetime is longest when the polarization corresponds to the largest estimated scattering rate. This observation allow us to exclude direct absorption of the trap light as the main loss mechanism.

Finally, to check how precisely the magnetic field is controlled, we set the magnetic field along the direction of light propagation. In this experiment, the magnetic field was codirected with the ODT beam and $\theta_k = 0^\circ$, $\theta_p = 90^\circ$; thus, rotation of the light polarization does not change polarizability at all. The ODT linear light polarization was rotated using a $\lambda/2$ plate. As one can see from Fig. 3(d), indeed the measured polarization does not change when light polarization changes and it is equal to the expected value from Eq. (9).

D. Vector polarizability

As described above, with magnetic field aligned along beam propagation direction $\theta_k = 0^\circ$, tensor polarizability does not depend on light polarization anymore. Therefore, this configuration is perfect for measurements of the vector part of polarizability. Thus, to determine vector polarizability, the magnetic field (3.94 G at this experiment) was aligned along the beam propagation direction and the ODT light ellipticity parameter, $\varepsilon = |\vec{u}^* \times \vec{u}|$, as well as sign of light polarization (sign of $\cos[\theta_k]$) was varied. This was realized by rotation of the $\lambda/4$ plate placed into the ODT beam. The ellipticity parameter was measured at all points by PBS and was calculated as

$$\varepsilon = 2\frac{p}{1+p^2}$$
$$p = \sqrt{\frac{P_{\min 1}}{P_{\max 2}}}, \tag{10}$$

where $P_{\min 1}$ and $P_{\max 2}$ are the minimum and maximum of powers of the beam at two orthogonal orientations of PBS. The circular polarization was formed by the $\lambda/4$ plate; its sign

TABLE I. Polarizability of Tm atom near 532 nm.

Polarizability, real part	Simulated, polarizability, α^{theor} (a.u.)	Measured polarizability α^{expt} (a.u.)	Statistical uncertainty $\Delta\alpha_{\text{stat}}$ (a.u.)	Systematic uncertainty $\Delta\alpha_{\text{sys}}$ (a.u.)	Total uncertainty $\Delta\alpha_{\text{tot}}$ (a.u.)
Scalar	583	547	13	190	190
Tensor	−140	−145	14	51	53
Vector	684	676	24	240	240

was determined from an angle between the linear polarization of incoming light and the plate's fast axis.

As is shown in Fig. 4(a), using fitted data from (1) with $\theta_p = 90^o$, $\alpha_t = -145$ a.u., and keeping α_{sc} as a parameter produces almost the same scalar part of polarizability: $\alpha_{sc} = 561 \pm 19_{\text{stat}}$ a.u. and $\alpha_v = 678 \pm 24_{\text{stat}}$ a.u.

In order to relate the losses in the dipole trap to polarization, we also measured the dependence of the trap lifetime on the ellipticity parameter [see Fig. 4(b)]. Here, lifetime of the trap again (similarly to the tensor case) cannot be described easily in terms of the imaginary part but rather behaves like the real part.

The values of the atomic polarizability of the thulium atom, including systematics uncertainties (see Appendix C) are summarized in Table I. Details of calculations of polarizability and estimations of systematic error can be found in Appendix A and Appendix C, correspondingly.

IV. CONCLUSION

Vector, tensor, and scalar polarizabilities were measured in thulium atoms ground state near 532.07-nm wavelength; which is a particularly important wavelength for optical dipole traps with thulium atoms. Experimental values were compared to the theoretically calculated values and these were in nice agreement with each other. It was found that at this wavelength contributions of tensor and vector polarizability are quite significant and thus allowed for the formation of spin-dependent lattices. Besides this, the losses of the optical dipole trap had also been measured, and these losses demonstrated correlation with the real rather than the imaginary parts of polarizability.

ACKNOWLEDGMENTS

This research was supported by the Russian Science Foundation Grant No. 18-12-00266. We also thank Aubrey Sergeant for help with manuscript preparation.

APPENDIX A: POLARIZABILITY

Full atomic polarizability was calculated by summing the contributions of all known polarizabilities from the NIST database [15] and using formulas (4), (5), (6) from Ref. [21]. In the arbitrary case, angular dependence of the tensor part of polarizability is different from expression (1) and is given by [22]

$$f(\theta_k, \theta_p, \varepsilon) = 1 - (3/2)\sin(\theta_k)^2[1 + \sqrt{1-\varepsilon^2}\cos(2\theta_p)], \tag{A1}$$

where $f(\theta_k, \theta_p, \varepsilon)$ is function, determining the angular dependence. In formula (1) thus the coefficient in front of the tensor part of polarizability is the following:

$$\frac{3m_F^2 - F(F+1)}{F(2F-1)} \times \frac{-f(\theta_k, \theta_p, \varepsilon)}{2}. \tag{A2}$$

Equation (A1) leads to $f(\theta_p) = 1 - 3\cos(\theta_p)^2$ in the case of linearly polarized light $\varepsilon = 0$ with a wave vector perpendicular to the magnetic-field direction ($\theta_k = \pi/2$), and degenerates to $f = 1$ in the case of light propagating in the z direction ($\theta_k = 0$).

APPENDIX B: FITTING DETAILS

The profile of a sweeping beam is complex; therefore, to determine the waist the following trick was used. First, recorded 1D distribution was analyzed from the statistical point of view, treating the beam profile as a probability distribution. Its center of brightness position was estimated as

$$m = \sum_k k \times I_k \Big/ \sum_k I_k, \tag{B1}$$

and relative standard deviation was estimated as

$$\sqrt{\sum_k (k-m)^2 I_k \Big/ \sum_k I_k}, \tag{B2}$$

with I_k being the brightness of the bin number k. For Gaussian beam one could calculate that conventional waist definition corresponding to the $1/e^2$ level of power density is equal to two standard deviations in beam distribution, if treated statistically.

Indeed, normal distribution $P_{\text{norm}}(x)$ is

$$P_{\text{norm}}(x) = \frac{1}{\sigma\sqrt{2\pi}} e^{-[(x-\mu)^2/2\sigma^2]}, \tag{B3}$$

where σ is standard deviation and μ is mean value of the distribution. Therefore, comparing (15) and (3) one could see that

$$w = 2\sigma. \tag{B4}$$

Thus, we took as the definition of effective waist for beam with sweeping beam as two standard deviations of the beam profile, treated as probability distribution.

APPENDIX C: SYSTEMATIC UNCERTAINTY

The systematic uncertainty was estimated as follows:

$$\frac{\Delta\alpha_{\text{sys}}}{\alpha} = \sqrt{\left(\frac{\Delta w_{z\,sys}}{w_z}\right)^2 + \left(3\frac{\Delta w_{x\,sys}}{w_x}\right)^2 + \left(\frac{\Delta P_{\text{sys}}}{P}\right)^2}.$$

We estimate a power uncertainty of 2%. However, the uncertainty in measuring waists (about 11%) made a major contribution to systematic uncertainty. Summing up all sources of uncertainty, the final systematic uncertainty for the measured scalar, tensor, and vector polarization is about 35%.

[1] D. Jaksch, C. Bruder, J. I. Cirac, C. W. Gardiner, and P. Zoller, Phys. Rev. Lett. **81**, 3108 (1998).

[2] M. Greiner and S. Fölling, Nature (London) **453**, 736 (2008).

[3] I. M. Georgescu, S. Ashhab, and F. Nori, Rev. Mod. Phys. **86**, 153 (2014).
[4] J. Dalibard, in *Proceedings of International School of Physics "Enrico Fermi"*, edited by M. Inguscio, S. Stringari, and C. E. Wieman, Vol. 140: Bose-Einstein Condensation in Atomic Gases (IOS Press, Amsterdam, 1999), pp. 321–349.
[5] A. Petrov, E. Tiesinga, and S. Kotochigova, Phys. Rev. Lett. **109**, 103002 (2012).
[6] S. Kotochigova, Rep. Prog. Phys. **77**, 093901 (2014).
[7] M. Lu, N. Q. Burdick, S. H. Youn, and B. L. Lev, Phys. Rev. Lett. **107**, 190401 (2011).
[8] J. Stuhler, A. Griesmaier, T. Koch, M. Fattori, T. Pfau, S. Giovanazzi, P. Pedri, and L. Santos, Phys. Rev. Lett. **95**, 150406 (2005).
[9] A. Griesmaier, J. Stuhler, T. Koch, M. Fattori, T. Pfau, and S. Giovanazzi, Phys. Rev. Lett. **97**, 250402 (2006).
[10] S. Baier, D. Petter, J. H. Becher, A. Patscheider, G. Natale, L. Chomaz, M. J. Mark, and F. Ferlaino, Phys. Rev. Lett. **121**, 093602 (2018).
[11] M. Wenzel, F. Böttcher, J.-N. Schmidt, M. Eisenmann, T. Langen, T. Pfau, and I. Ferrier-Barbut, Phys. Rev. Lett. **121**, 030401 (2018).
[12] M. Lepers, J.-F. Wyart, and O. Dulieu, Phys. Rev. A **89**, 022505 (2014).
[13] J. H. Becher, S. Baier, K. Aikawa, M. Lepers, J.-F. Wyart, O. Dulieu, and F. Ferlaino, Phys. Rev. A **97**, 012509 (2018).
[14] V. V Tsyganok, V. A. Khlebnikov, E. S. Kalganova, D. A. Pershin, E. T. Davletov, I. S. Cojocaru, I. A. Luchnikov, A. V Berezutskii, V. S. Bushmakin, V. N. Sorokin, and A. V. Akimov, J. Phys. B At. Mol. Opt. Phys. **51**, 165001 (2018).
[15] A. Kramida, Y. Ralchenko, J. Reader, and NIST ASD Team, NIST Atomic Spectra Database (Version 5.6.1), https://physics.nist.gov/asd (2018).
[16] N. L. Manakov, V. D. Ovsiannikov, and L. P. Rapoport, Phys. Rep. **141**, 320 (1986).
[17] V. Tsyganok, D. Pershin, V. Khlebnikov, E. Davletov, and A. Akimov, JETP **128**, 199 (2019).
[18] D. A. Pershin, V. V. Tsyganok, V. V. Yaroshenko, V. A. Khlebnikov, E. T. Davletov, E. L. Svechnikov, V. N. Sorokin, P. V. Kapitanova, and A. V. Akimov, Bull. Lebedev Phys. Inst. **45**, 377 (2018).
[19] R. Grimm, M. Weidemüller, and Y. B. Ovchinnikov, Adv. At. Mol. Opt. Phys. **42**, 95 (2000).
[20] D. V. Sheludko, S. C. Bell, R. Anderson, C. S. Hofmann, E. J. D. Vredenbregt, and R. E. Scholten, Phys. Rev. A **77**, 033401 (2008).
[21] D. Sukachev, S. Fedorov, I. Tolstikhina, D. Tregubov, E. Kalganova, G. Vishnyakova, A. Golovizin, N. Kolachevsky, K. Khabarova, and V. Sorokin, Phys. Rev. A **94**, 022512 (2016).
[22] P. G. Westergaard, J. Lodewyck, L. Lorini, A. Lecallier, E. A. Burt, M. Zawada, J. Millo, and P. Lemonde, Phys. Rev. Lett. **106**, 210801 (2011).